

## Effects of silica nanoparticles on enhancing the specific heat capacity of carbonate salt eutectic (work in progress)

Donghyun Shin and Debjyoti Banerjee

Texas A&M University, College Station, TX, USA

*This paper is dedicated to Prof. K.R. Rajagopal's 60<sup>th</sup> birthday.*

---

### Abstract

Nanomaterials were obtained by dispersing silica nanoparticles in eutectic salt mixtures. The synthesis protocol was varied to obtain different nanomaterial samples of the same composition but different morphologies. The synthesis protocols that led to agglomerated nanoparticles resulted in coarse powders (Type-A samples) and the protocols that led to (un-agglomerated) well dispersed nanoparticles resulted in fine grained powders (Type-B samples). Measurements using differential scanning calorimeter (DSC) showed that the average specific heat capacity of the Type-A samples was enhanced by ~20 % (solid phase) and ~75 % (liquid phase); while that of Type-B samples was enhanced by ~34 % (solid phase) and ~100 % (liquid phase). Electron microscopy of the samples revealed that the variation in the thermophysical properties of the different samples was caused by the amount of the agglomeration of the nanoparticles as well as the formation of compressed phase. This study shows that these nanomaterials can enable significant reduction in the cost of solar thermal power.

---

### 1. Introduction

#### 1.1. Solar Thermal Energy Storage

Concentrated Solar Power (CSP) technology involves the collection of solar energy from large areas and focusing the energy into a small space by using solar collectors (mirrors) or lenses. Heat Transfer Fluid (HTF) is typically used to transfer the harvested energy into Thermal Energy Storage (TES) devices. Thermodynamic cycles (such as Rankine or Stirling cycle) are utilized to generate power from the stored thermal energy. Thus TES enables power generation during periods of interruption in solar irradiation (e.g., due to cloud cover during daytime or during nighttime) or to supply power to the electric grid system during periods of peak demand. The thermodynamic efficiency of the CSP system therefore depends on the operating temperature of the TES. The operating temperature of the conventional TES units is restricted to ~ 400 °C due to the thermal decomposition temperatures of the organic materials that are currently used in these devices, e.g., mineral oil, fatty acid, or paraffin wax (Kearney et al., 2003). Molten salts are compatible for the operation of the TES devices at higher temperatures.

Typical molten salt materials include alkali-carbonate, alkali-nitrate, alkali-chloride, or their eutectic. These materials are thermally stable at high temperatures, i.e., exceeding 600 °C (Janz et al., 1979). Using the molten salts as TES materials confer several benefits: (1) Higher thermodynamic efficiency enables the cost of solar thermal power to be reduced significantly (thermodynamic efficiency can be increased from 54% to 63%, when the TES operating temperature is increased from 400 °C to 560 °C, where 560 °C corresponds to the start of creep temperature of stainless steel). (2) Molten salts are cheap and environmentally safe compared to conventional materials used for TES. This significantly reduces the material cost as well as potential environmental cost.

However, the poor thermo-physical properties (e.g., specific heat capacity less than ~2 J/g-K and thermal conductivity less than ~1 W/m-K) of these salts may increase the size requirement of TES. This may defeat the cost-reductions realized by the higher operating temperatures (higher thermodynamic efficiency) and low material costs afforded by the choice of these materials. The thermophysical property values can be enhanced by doping these salts with minute concentration of nanoparticles. In this study the solid phase of the synthesized nanomaterials will be termed as “nanocomposites” and the liquid phase will be termed as “nanofluids”.

### 1.2. Nanocomposites and Nanofluids

Colloidal suspension of nanometer-sized particles dispersed in a solvent material is termed as a “nanofluid” (Choi, 1995). Various nanofluids and nanocomposites have been reported for their anomalous enhancement in the effective thermal conductivity. The thermal conductivity of polymer materials was enhanced by 30% when mixed with carbon nanotube (CNT) at 1% mass fraction (Wang et al., 2010). The thermal conductivity of epoxy was enhanced by 100% when mixed with Carbon Nanotube (CNT) at 1.5 % mass fraction (Song and Youn, 2005). The thermal conductivity of high density polyethylene (HDPE) was enhanced by 700 % when mixed with CNT at 20% by volume (Haggenmueller et al., 2007). The thermal conductivity of ethylene glycol (EG) was enhanced by 40% when mixed with Cu nanoparticles at 0.3 % by volume (Eastman et al., 2001). The thermal conductivity of EG was enhanced by 20% when mixed with CuO nanoparticles at 4 % concentration by volume (Lee et al., 1999). The thermal conductivity of oil (poly-alpha-olefin/ PAO) was enhanced by 150% when mixed with CNT at 1 % by volume (Choi et al., 2001). Several transport mechanisms reported in the literature in an attempt to comprehend the observed anomalous enhancement of the thermal conductivity include: Brownian motion of the nanoparticles (that induces nano-scale convection), ordered liquid molecules on the surface of nanoparticles to form a semi-solid layer of the solvent molecules, and enhanced interfacial thermal resistance between the nanoparticles and the surrounding solvent material (Kebllinski et al., 2002; Jang and Choi, 2004; Prasher et al., 2006). In recent studies it has been proposed that the formation of percolation networks due to aggregation of nanoparticles can also enhance the thermal conductivity of the nanomaterials (Kebllinski et al., 2008; Evans et al., 2008).

Similarly, specific heat capacity ( $C_p$ ) of a material can be also enhanced by mixing with nanoparticles. Several studies reported decrease of the specific heat capacity of aqueous nanofluids. (Zhou and Ni, 2008; Vajjha and Das, 2009) In contrast, enhancement of the specific heat capacity has been reported for non-aqueous nanofluids. The  $C_p$  of PAO was enhanced by 50% when mixed with graphite nanoparticles at 0.6 % mass fraction (Nelson et al., 2009). The  $C_p$  of  $\text{Li}_2\text{CO}_3\text{-K}_2\text{CO}_3$  eutectic salt was enhanced by 26% when mixed with silica nanoparticles at 1 % mass fraction (Shin and Banerjee, 2011). The  $C_p$  of  $\text{Li}_2\text{CO}_3\text{-K}_2\text{CO}_3$  eutectic salt was enhanced by 19% when mixed with CNT at 1 % mass fraction (Shin et al., 2010).

### 1.3. Objective of Study

The objective of the study was to explore the effect of addition of silica nanoparticles on the specific heat capacity of the eutectic salt. The effect of the synthesis protocol on the specific heat capacity of the nanomaterials was also explored in this study. The motivation of this study was to synthesize novel nanomaterials for TES in CSP applications. Eutectic of lithium carbonate and potassium carbonate (62:38 by molar ratio) was chosen for its stability at high temperatures (exceeding 600 °C). The melting point of the eutectic is 488 °C. Two samples were synthesized using a liquid solution method. One of the methods involved a refinement step to remove agglomerated nanoparticles from the samples. A differential scanning calorimeter (DSC; Q20, TA instruments) was used to measure the  $C_p$  of the samples. Simple mixing rule (Model 1, Equation 1) was used to estimate the property values for the mixture (nanomaterials), as follows:

$$C_{p,t} = \frac{m_{np}C_{p,np} + m_b C_{p,b}}{m_{np} + m_b} \quad (1)$$

where  $C_p$  is specific heat and  $m$  is mass (or mass fraction) of the sample. Subscript  $t$ ,  $np$ , and  $b$  denote property values of the mixture (nanomaterial), nanoparticle, and pure solvent material (eutectic). This equation is frequently used in nanofluids literature (e.g., Vajjha and Das, 2009; Zhou and Ni, 2008). Transmission Electron Microscopy (TEM; Jeol JEM-2010) was used for materials characterization and to verify the agglomeration of the nanoparticles.

## 2. Experiment

### 2.1. Synthesis Protocol

Two synthesis methods were explored in this study. Lithium carbonate and potassium carbonate was procured from Sigma Aldrich, Co. Silica nanoparticles were procured from Meliorum Tech. Nominal size of the nanoparticles was reported to be ~ 10 nm by the manufacturer. The actual size of the nanoparticles was measured by TEM to vary from ~1-20 nm. (This will be discussed later in the paper). The concentration of the nanoparticles is fixed at 1.5 % by weight, for comparison with the previous results (Shin and Banerjee, 2011; Shin et al., 2010). The two synthesis protocols are shown in Figure 1 and briefly described as follows: 3.0 mg of the silica nanoparticles and 197.0 mg of the

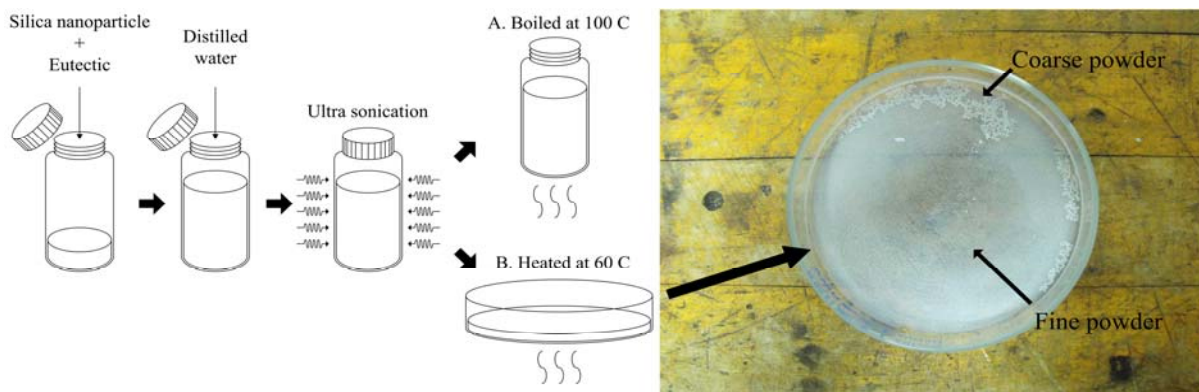


Figure 1. (a) Schematic for the two protocols explored in this study for synthesis of nanomaterials.

(b) Image showing the petri-dish after complete evaporation showing the coarse and fine powder regions.

eutectic of the molten salt were mixed in a glass bottle (25 ml). The mixture was dissolved in 20 ml of distilled water. The solution was ultra-sonicated for 200 minutes (Branson 3510, Branson Ultrasonics Co.). After the sonication, the water was evaporated from the aqueous solution using two different protocols, shown in Figure 1 (the evaporation in both protocols was performed in a glove box with filtered air circulation to minimize contamination):

- (A) The glass bottle was placed on a hot plate and the solution was maintained at a temperature of 100 °C to rapidly evaporate the water by boiling (the resulting salt mixture is called Type-A sample).
- (B) The water solution in the glass bottle was poured on a glass petri-dish. The petri-dish was placed on a hot plate and the solution temperature was maintained at 60 °C (Since boiling was observed to enhance the agglomeration of the nanoparticles, the evaporation temperature was significantly reduced to 60 °C in order to reduce the agglomeration of the nanoparticles). The water was evaporated rapidly and complete evaporation was accomplished in 30 minutes. Variation in the concentration of water in different parts of the petri-dish as the evaporation progressed caused the formation of finely dispersed salt powder during the initial stages of the evaporation along the periphery of the petri-dish (where the nanoparticles were found to be un-agglomerated and dispersed uniformly). Evaporation of the water in the final stages of the process from the center of the petri-dish led to the formation of coarse powder of the salts (where the nanoparticles were found to be agglomerated and precipitated/ segregated from the eutectic material). The finely dispersed powder was selectively scraped off from the petri-dish (“Type-B” samples).

### 2.1. Measurement of Specific Heat Capacity

The  $C_p$  measurement was performed using standardized DSC testing protocol (ASTM-E1269). Tzero hermetic pan/lid (TA instruments) was used to place the samples in the DSC. The sample mass ranged from ~15 - 20 mg. A custom automated temperature protocol was implemented for performing the measurements. The sample was initially maintained at 150 °C for 10 minutes to achieve steady state conditions. The sample was then heated up to 560 °C at a fixed rate (20 °C / minute) and the heat flux was monitored as a function of temperature. The sample was then maintained at 560 °C for another 10 minutes to ensure steady state conditions. Each sample was subjected to repeated freeze/ thaw cycles ~4-6 times to ensure repeatability of the measurements and to ensure the stability of the nanoparticles in the mixture. A sapphire standard (25.938 mg), was subjected to the thermo-cycle protocol and the heat flux was recorded as a function of temperature. The specific heat of the sample was then computed by comparing the heat flux and the weight of the sample to that of the sapphire standard.

## 3. Results and Discussion

### 3.1. Specific Heat Capacity Data

The  $C_p$  measurements for the Type-A and Type-B samples are shown in Tables 1 and Figures 2-3. Table 1 and Figure 2 show the  $C_p$  of the Type-A and Type-B nanocomposites (solid phase, ~350 °C - 450 °C). It was observed that the  $C_p$  of

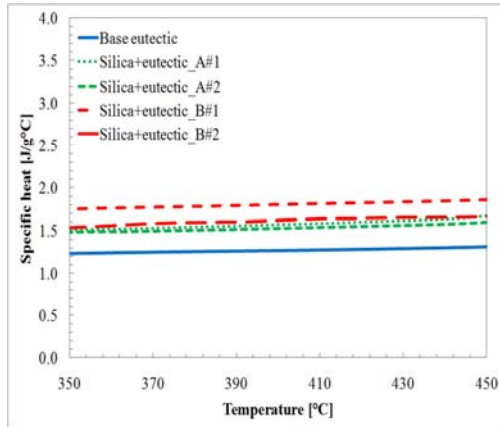


Figure 2. Variation of specific heat capacity with temperature for pure eutectic sample and nanocomposite samples (solid phase data).

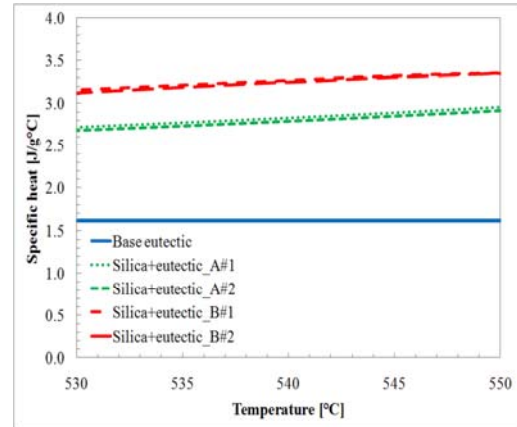


Figure 3. Variation of specific heat capacity with temperature for pure eutectic sample and nanofluid samples (liquid phase data).

the Type-A nanocomposites was enhanced by 22 % compared to that of the pure eutectic, while the  $C_p$  of the Type-B nanocomposite (after refinement procedure to remove the agglomerated nanoparticles) was enhanced by 42 % over that of the pure eutectic. Table 1 and Figure 3 shows the  $C_p$  of the Type-A and Type-B nanofluids (between 525 and 555°C). The  $C_p$  of the Type-A nanofluids was enhanced by 74 %, while that of the Type-B nanofluids was enhanced by 101 %. To verify the accuracy of the measurements, the  $C_p$  of the pure eutectic was measured and compared with the literature data. The  $C_p$  of the pure eutectic in the liquid phase is measured to be 1.619 J/g-K, which is consistent with the literature data of 1.6 J/g-K (Araki et al., 1988), showing that the experimental error is ~1.2 %.

Model 1 failed to predict the enhanced specific heat of the nanocomposites as well as the nanofluids. Figure 4 shows the predictions from Model 1 compared with the experimental data for the pure eutectic samples and the nanomaterial samples. Since the specific heat capacity of the nanoparticles is lower than that of the pure eutectic, the estimate by Model 1 was slightly lower than that of the pure eutectic. This implies that Model 1 cannot be used to predict the specific heat capacity of these nanomaterials.

Table 1. Specific heat capacity of pure eutectic, Type-A and Type-B nanocomposite (solid phase data) and nanofluid samples (liquid phase data). Measurement uncertainty is ~1.3- 4.1 %

Specific Heat (J/g-K)	Pure Eutectic	Nanomaterial-A#1	Nanomaterial-A#2	Nanomaterial-B#1	Nanomaterial-B#2
Solid phase	1.276	1.586	1.537	1.812	1.626
(Enhancement %)	(NA)	(24 %)	(20 %)	(42 %)	(27 %)
Error %	3.3 %	1.5 %	1.3 %	2.8 %	1.5 %
Liquid phase	1.619	2.836	2.794	3.260	3.240
(Enhancement %)	(-)	(75 %)	(73 %)	(101 %)	(100 %)
Error %	4.0 %	1.3 %	1.9 %	4.1 %	3.3 %

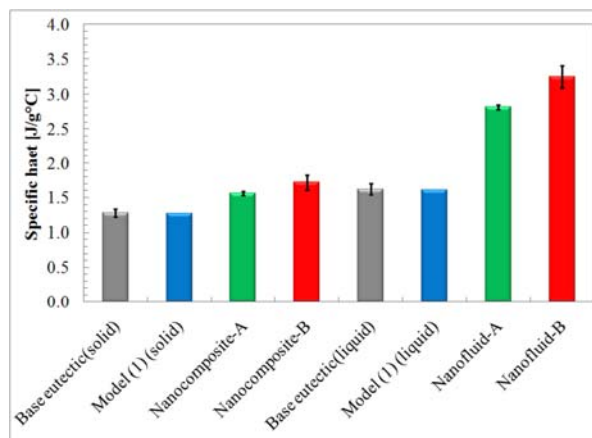


Figure 4. Comparison of experimental data with predictions from Model 1.

### 3.2. Materials Characterization Using Electron Microscopy

Since specific heat capacity depends on the material composition and morphology (structure), materials characterization of the nanomaterial samples was performed using TEM. Figure 5 shows the TEM images of the nanocomposite. TEM images showed that the Type-B samples formed needle-shaped structures within the solvent material – demonstrating that the nanoparticles induce phase transformation (formation of “compressed phase”) within the solvent material. The compressed phase is expected to have different thermal properties than the bulk eutectic material. The compressed phase is expected to contribute a significant proportion of the specific heat capacity enhancement.

Nanoparticles tend to agglomerate and consequently segregate from the eutectic, as shown in Figure 1 (b). Hence, it is necessary to verify if the nanoparticles were agglomerated in both samples. Figure 6 shows a representative TEM image of the type-A and Type-B samples. It was observed that the nanoparticles were not agglomerated yet well distributed in the eutectic for Type-B samples. For Type-A samples the nanoparticles were observed to be bigger in size (possibly due to agglomeration) and not as uniformly distributed.

### 3.3. Discussions

The anomalous enhancement of the specific heat capacity values of the nanomaterials is not predicted by the simple mixing model (Model 1). The enhancement of the specific heat capacity values in this study may arise from similar transport mechanisms that are also responsible for the thermal conductivity enhancement of nanomaterials - or it may be due to other factors (e.g., due to availability of additional degrees of freedom due to phase transformation caused by the nanoparticles – that manifests itself by the resulting formation of the needle shaped micro / nano-structures). The needle-shaped structures within the solvent material (as shown in Figure 5) are expected to be one of the dominant factors, which contributes a significant proportion of the enhancement in the specific heat capacity of the nanomaterials.

Reports in the literature show that liquid molecules acquire an ordered structure in vicinity of the surface of the nanoparticles, essentially mimicking the underlying lattice structure, leading to the formation of a dense semi-solid layer (Oh et al., 2005). This dense semi-solid layer of the solvent molecules is called the “compressed phase”. The nanoparticle thus nucleates the compressed phase which is ~ 1nm in thickness. This compressed phase can subsequently grow to form larger size micro-structures which appear as needle shaped features in the TEM images, as shown in Figure 5. The needle shaped structures can form a percolation network which is expected to have enhanced thermal properties than the bulk solvent material. The nucleation and growth of the compressed phase, thus manifests effectively as the enhancement in the specific heat capacity of the nanomaterials.

The mass fraction of the nucleated compressed phase is expected to be proportional to the surface area of the nanoparticles. This can help to explain the difference in the enhancement between the Type-A and Type-B samples. During the synthesis process, a certain amount of the agglomerated nanoparticles (which was segregated from the pure eutectic in the form of coarse powders) was removed from Type-B samples. In contrast, no refinement of the Type-A

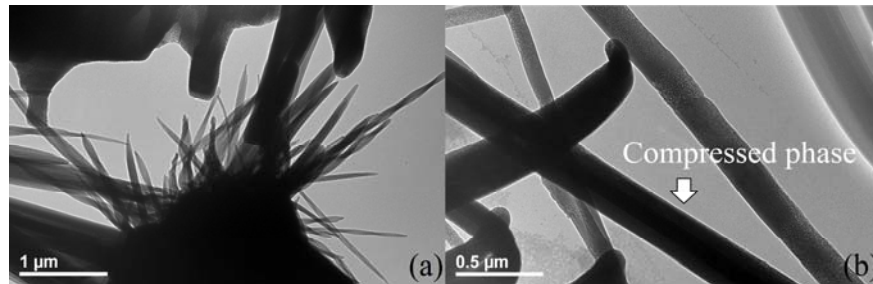


Figure 5. TEM images of the Type-B samples. Needle shaped structures (compressed phase) were induced within the solvent material by the nanoparticles, where the diameter of the needle shaped structures is  $\sim 200 - 400$  nm.

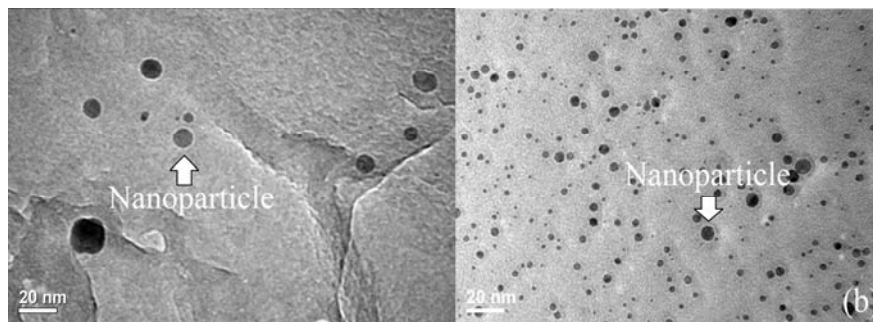


Figure 6. (a) TEM images of silica nanoparticles in the Type-A samples. (b) TEM images of the silica nanoparticles in the Type-B samples. Both images were obtained after multiple freeze/ thaw cycles from the thermo-cycling experiments performed in the DSC.

samples was performed. Therefore, the Type-B samples may have lower concentration of nanoparticle agglomerates (in comparison to Type-A samples where the agglomerates were not removed or the refinement procedure was not implemented). This means that the nanoparticles in the type-B samples will effectively have larger specific surface area (per unit mass of the nanoparticles) than that for the Type-A samples. This results in higher mass fraction of the compressed phase and therefore higher specific heat capacity of the Type-B samples.

#### 4. Conclusions

In this study, nanomaterials were synthesized using two different protocols. In the first synthesis process (Type-A sample) the nanomaterials contain a larger proportion of the agglomerated nanoparticles. In the second synthesis process (Type-B samples) the nanomaterial is refined to remove a portion of the agglomerated nanoparticles. In other words, the specific surface area (surface area per unit mass of the nanoparticles) for Type-A samples is smaller than that of the Type-B samples. The specific heat capacity measurements were performed using a Differential Scanning Calorimeter (DSC) and using an automated thermo-cycling procedure involving multiple freeze/ thaw cycles. The results show that the specific heat capacity of the Type-A samples was enhanced by 22 % (solid phase) and 74 % (liquid phase). The specific heat capacity of the Type-B samples was enhanced by 34 % (solid phase) and 101 % (liquid phase). TEM analyses of the samples showed the formation of needle shaped structures in Type-B samples which can lead to the formation of percolation networks of “compressed phase” within the solvent material. The needle-shaped structures formed by the compressed phase are expected to have higher specific heat capacity than the bulk eutectic and therefore contribute a significant proportion to the enhancement of the specific heat capacity that is observed for the nanomaterials. Since the mass fraction of the compressed phase and the formation of the percolation network are proportional to the specific surface area of the nanoparticles (surface area per unit mass of the nanoparticles), Type-B samples are expected to have higher specific surface area than that of the type-A samples. This was verified by the TEM images, where minimal agglomeration of the nanoparticles was observed in the Type-B samples compared to that of the Type-A samples.

These results have significant implications for their implementation in TES/ CSP systems. The observed enhancement of specific heat capacity by 100 % in the nanomaterials can enable the reduction in the cost of solar thermal power by 50%, due to a combination of higher operating temperatures (therefore higher thermodynamic efficiencies) and lower material requirements (therefore, lower material costs).

### Acknowledgments

The authors acknowledge the support of the Department of Energy (DOE) Solar Energy Program (Golden, CO) under Grant No. DE-FG36-08GO18154 (Title: “Molten Salt-Carbon Nanotube Thermal Energy Storage For Concentrating Solar Power Systems”). This paper is dedicated to Prof. K.R. Rajagopal’s 60<sup>th</sup> birthday.

### References

- Araki, N., Matsuura, M., Makino, A., Hirata, T. & Kato, Y. 1988 Measurement of thermophysical properties of molten salts: Mixtures of alkaline carbonate salts, *International Journal of Thermophysics* 9, 1071-1080.
- Choi, S. U. S. 1995 Enhancing thermal conductivity of fluids with nanoparticles. In *Proc. developments and applications of non-newtonian flows* (ed. D. A. Siginer & H. P. Wang), FED-Vol. 231/MD-Vol. 66, pp. 99–105. ASME, New York.
- Choi, S. U. S., Zhang, Z. G., Yu, W., Lockwood, F. E. & Grulke, E. A. 2001 Anomalous thermal conductivity enhancement in nanotube suspensions, *Appl. Phys. Lett.* 79, 2252-2254.
- Eastman, J. A., Choi, S. U. S., Li, S., Yu, W. & Thompson, L. J. 2001 Anomalous increased effective thermal conductivities of ethylene glycol-based nanofluids containing copper nanoparticles, *Appl. Phys. Lett.* 78, 718-720.
- Evans, W., Prasher, R., Fish, J., Meakin, P., Phelan, P. & Keblinski, P. 2008 Effect of aggregation and interfacial thermal resistance on thermal conductivity of nanocomposites and colloidal nanofluids, *International Journal of Heat and Mass Transfer* 51, 1431-1438.
- Haggenmueller, R., Guthy, C., Lukes, J. R., Fischer, J. E. & Winey, K. I. 2007 Single wall carbon nanotube / polyethylene nanocomposites: *thermal and electrical conductivity*, *Macromolecules* 40, 2417-2421.
- Jang, S. P., and Choi, S. U. S. 2004 Role of Brownian motion in the enhanced thermal conductivity of nanofluids, *Appl. Phys. Lett.* 84, 4316-4318.
- Janz, G., Allen, C., Bansal, N., Murphy, R. & Tomkins, R. 1979 Physical Properties Data Compilations Relevant to Energy Storage, U. S. Dept. of Commerce, *National Bureau of Standards*, Washington, DC.
- Kearney, D., Herrmann, U., Nava, P. & Kelly, B. 2003 Assessment of a molten salt heat transfer fluid in a parabolic trough solar field, *J. Sol. Energy Eng.* 125, 170-176.
- Keblinski, P., Phillpot, S. R., Choi, S. U. S. & Eastman, J. A. 2002 Mechanisms of heat flow in suspensions of nano-sized particles (nanofluids) *Int. J. Heat Mass Transfer* 45, 855-863.
- Keblinski, P., Prasher, R. & Eapen, J. 2008 Thermal conductance of nanofluids: is the controversy over? *Journal of Nanoparticle Research* 10, 1089-1097.
- Lee, S., Choi, U. S., Li, S. & Eastman, J. A. 1999 Measuring Thermal Conductivity of Fluids Containing Oxide Nanoparticles, *ASME J. Heat Transfer* 121, 280-289.
- Nelson, I. C., Banerjee, D. & Ponnappan, R. 2009 Flow loop experiments using polyalphaolefin nanofluids, *Journal of Thermophysics and Heat Transfer* 23, 752-761.
- Oh, S. H., Kauffmann, Y., Scheu, C., Kaplan, W. D. & Rühle, M. 2005 Ordered liquid aluminum at the interface with sapphire, *Science* 310, 661-663.
- Prasher, R., Bhattacharya, P. & Phelan, P. E. 2006 Brownian-motion-based convective-conductive model for *the effective thermal conductivity of nanofluids* *J. Heat Transfer* 128, 588-595.
- Shin, D. and Banerjee, D. 2011 *Enhanced specific heat of silica nanofluid*, *J. Heat Transfer* 133,024501.
- Shin, D., Jo, B., Kwak, H. & Banerjee, D. 2010 Investigation of high temperature nanofluids for solar thermal power conversion and storage applications, in *Proc. international heat transfer conf. IHTC14*, ASME, Washington, DC, USA.
- Song, Y.S., and Youn, J.R., 2005. Influence of dispersion states of carbon nanotubes on physical properties of epoxy nanocomposites, *Carbon*, 43, 1378-1385.
- Vajjha, R. S., and Das, D. K. 2009 Specific heat measurement of three nanofluids and development of new correlations, *J. Heat Transfer* 131, 071601.
- Wang, J., Xie, H., Xin, Z., Li, Y. & Chen, L. 2010 Enhancing thermal conductivity of palmitic acid based phase change materials with carbon nanotubes as fillers. *Solar Energy* 84, 339-344.
- Zhou, S., and Ni, R. 2008 Measurement of the specific heat capacity of water-based AIO nanofluid, *Appl. Phys. Lett.* 92, 093123.